Periodic coupling inhibits second-order consensus on networks

Fabian Baumann,[1,*] Igor M. Sokolov,[1,2] and Melvyn Tyloo[3]
[1]*Institut für Physik, Humboldt-Universität zu Berlin, Newtonstraße 15, 12489 Berlin, Germany*
[2]*IRIS Adlershof, Humboldt-Universität zu Berlin, Zum Großen Windkanal 6, 12489 Berlin, Germany*
[3]*School of Engineering, University of Applied Sciences of Western Switzerland HES-SO, CH-1951 Sion, Switzerland*

(Received 18 August 2020; accepted 28 October 2020; published 23 November 2020)

Consensus algorithms on networks have received increasing attention in recent years for various applications, ranging from distributed decision making to multivehicle coordination. In particular, second-order consensus models take into account the Newtonian dynamics of interacting physical agents. For this model class, we uncover a mechanism inhibiting the formation of collective consensus states via rather small time-periodic coupling modulations. We treat the model in its spectral decomposition and find analytically that, for certain intermediate coupling frequencies, parametric resonance is induced on a network level—at odds with the expected emergence of consensus for very short and long coupling time scales. Our formalism precisely predicts those resonance frequencies and links them to the Laplacian spectrum of the static backbone network. The excitation of the system is furthermore quantified within the theory of parametric resonance, which we extend to the domain of networks with time-periodic couplings.

DOI: 10.1103/PhysRevE.102.052313

I. INTRODUCTION

Decentralized collective dynamics arise in a variety of different contexts, where single units interact *without* a centralized authority controlling the overall process. Often such interactions are modeled using networks. Depending on the context, the information flow between two network nodes may be interpreted differently—ranging from single neurons coupled via action potentials [1,2], to animal groups exchanging cues on prey or predators [3,4], to communicating robots within vehicular platoons [5–8]. Notably, it has been shown that for many coupled dynamical systems the arising collective states strongly depend on the underlying network topology [9].

Traditionally, special attention has been paid to the emergence of *consensus* [10–12]. The outstanding role of consensus states for many systems is often justified by collective decision making, which requires agreement on a population level to achieve a collective goal [11]. For example, fish schools have been shown to reach increased levels of collective sensitivity if individuals are strongly aligned, which corresponds to a consensus on the heading direction [13]. In social systems, language-based communication relies on sets of quasistatic vocabularies, where a consensus on the meaning of a word has been established [14]. In vehicular platoons, consensus is often attributed to situations in which all involved robotic vehicles are located at the same position, point in the same direction, or move at the same speed [5–7,15,16].

To model consensus on networks, most previous studies considered so-called first-order systems, which neglect the inertia of individual units (or agents) (see [15,17] for extensive reviews). These approaches rely on the linear assimilation process

$$\dot{x}_i = -\sum_j A_{ij}(x_i - x_j),$$

which is based on a diffusive coupling between the states of nearest neighbors (e.g., their positions) x_i and x_j. The network of interactions is encoded in the elements of the adjacency matrix, where $A_{ij} = 1$ if i and j interact, and $A_{ij} = 0$ otherwise. In first-order systems consensus is reached if $|x_i - x_j| = 0, \forall i, j$, which yields $\dot{x}_i = 0, \forall i$.

To describe more realistically the formation of consensus among physical objects, linear second-order models have been developed. They take into account the Newtonian dynamics of single agents by a second-order time derivative [15,18–27], i.e.,

$$\ddot{x}_i = -\sum_j A_{ij}[(x_i - x_j) + \mu(\dot{x}_i - \dot{x}_j)].$$

In addition to the diffusive coupling between agents' positions (x_i's), such models implement a mechanism for velocity alignment, which leads to consensus if $\mu > 0$ is sufficiently large [15]. States of consensus are defined as $|x_i - x_j| = 0$ and $|\dot{x}_i - \dot{x}_j| = 0 \ \forall \ i, j$, such that agents' velocities do generally not vanish if consensus is reached. Such models have been studied extensively both in discrete and in continuous time [15,18–27] and have been applied to various problems ranging, in particular, from leader-follower control [27], to flocking [16], to multivehicle coordination [19], where, more specifically, the effects of limited interaction ranges [26], time delays [20], and different networks for position and velocity coupling [25] were investigated. With regard to the underlying interaction topology, it was shown that networks with a

*Corresponding author: fabian.olit@gmail.com

 ©2020 American Physical Society

(directed) spanning tree do not yield a sufficient condition for achieving consensus in second-order systems [28]—at odds with their first-order counterparts.

While the vast majority of consensus research focused on static networks [15,18–27], less attention has been paid to the effects arising on temporal, i.e., time-varying, networks. Exceptions include investigations of multiagent systems on a switching topology [21,22], where the interaction network changes in discrete steps. In contrast to first-order systems, it was found that consensus is not necessarily achieved if infinitely many unions of consecutive network snapshots have a directed spanning tree [22]. A further type of time-varying networks has been investigated for the synchronization of nonlinear oscillators. Although the underlying mechanism is different, and may give rise to phase transitions [29,30], the synchronized states found in such systems are similar to those arising in linear consensus models [31]. Specifically, [32,33] considered a network with time-periodic coupling strengths, while the underlying backbone topology does not change. Interestingly, it was found that such a coupling modulation may strongly impact the synchronization behavior of the considered systems. In [33], using the classical Rössler oscillator, network synchronizability could be significantly improved by tuning the coupling frequency. In contrast, the same periodic coupling was found to suppress synchronization in ensembles of globally coupled first-order Kuramoto oscillators [32].

Inspired by these studies, in this paper, we uncover yet another mechanism inhibiting the formation of collective consensus states on networks. It is induced not by a switching network topology [21,22], but by the time-periodic coupling modulation, as proposed in [32,33]. To this end, we consider a general second-order model, as proposed in [34], for two different settings: (i) with (viscous) damping and without velocity alignment [damped oscillator (DO)] [35] and (ii) without damping and with velocity alignment [second-order consensus (SOC)], where the latter corresponds to the traditional second-order consensus model [18–20,23–26]. For both model versions, the interaction strengths are periodically modulated around well defined mean values which are encoded in a static and symmetric backbone network. In the limits of very fast and very slow modulations, we find that global consensus states emerge—as expected for the time-averaged static connectivity [19]. Interestingly, however, specific intermediate modulation frequencies lead to an excitation of the system, and thereby inhibit the formation of a global consensus.

As we demonstrate, this collective dynamical phenomenon can be understood in terms of parametric resonance [36]. On the level of network modes, it is revealed by the spectral decomposition of the system. In our analysis we link the corresponding resonance frequencies (of such parametric oscillators) to the Laplacian spectrum of the static backbone network. We furthermore estimate the growth rates of oscillation amplitudes in the case of resonance. As we will briefly discuss in the Appendix, using the Kuramoto model [37] with inertia [38–40], our framework may also be applied to nonlinearly coupled systems close to a synchronized fixed point.

The rest of the paper is structured as follows. In Sec. II we introduce the considered model. Using a spectral decomposition we derive decoupled mode equations, which can be treated within the theory of parametric oscillators. This allows us to link the resonance frequencies of both model versions (DO and SOC) to the Laplacian spectrum of the backbone matrix. In Sec. III we validate and complement our theoretical considerations using numerical simulations on different networks, and briefly discuss the theory's applicability to nonlinearly coupled oscillators (see the Appendix). The paper is summarized and concluded in Sec. IV.

II. MODEL AND THEORY

Let us consider a network of n coupled agents. The matrix which encodes the coupling strengths between two agents, $\mathbf{W}(t) = f(t)\mathbf{A}$, is composed of two parts: (i) a static and symmetric backbone network, described by the adjacency matrix $\mathbf{A}$, and (ii) the periodic modulation function [32,33]

$$f(t) = 1 + h\sin(\omega t), \tag{1}$$

with frequency ω and amplitude h. If two agents i and j are connected, it is encoded as $A_{ij}(=A_{ji}) = 1$, and as $A_{ij}(=A_{ji}) = 0$ otherwise. To exclude repulsive coupling we assume $h \in [0, 1]$ in the following. Note that due to the periodicity of $f(t)$ the network backbone and the coupling matrix are connected via the temporal average $\mathbf{A} = \lim_{T\to\infty} T^{-1}\int_0^T \mathbf{W}(t)dt$. Each agent i is associated with a distinct node of the network and is characterized by a time-dependent state variable, $x_i(t)$, where we will omit the time dependence for brevity in the following.

To model the collective dynamics we consider the established model for second-order consensus on networks [18–20,23–26], where we additionally assume time-periodic couplings. In its most general form including dissipation [41], it is described by the following set of second-order differential equations:

$$\begin{aligned}\ddot{x}_i + d(t)\,\dot{x}_i = &-\gamma\sum_{j=1}^{n} W_{ij}(t)\,(x_i - x_j)\\ &-\mu\sum_{j=1}^{n} W_{ij}(t)\,(\dot{x}_i - \dot{x}_j),\end{aligned} \tag{2}$$

where $W_{ij}(t)$ is the ijth element of the symmetric coupling matrix $\mathbf{W}$ at time t, and $d(t)$ denotes the damping coefficient. The coefficients $\gamma, \mu > 0$ control the strengths of diffusive coupling between the agents' positions [first sum on the right-hand side of Eq. (2)] and velocities (second sum), respectively.

In the first case, the DO model, we assume that each agent dissipates energy ($d > 0$), and agents are not coupled with respect to their velocities ($\mu = 0$). This corresponds to an ensemble of n one-dimensional damped harmonic oscillators coupled via linear springs with time-dependent spring constants $\gamma W_{ij}(t)$. Similar harmonic oscillators, with time-invariant couplings, have been investigated on networks using the classical mass spring model [35]. More importantly, however, the DO model describes the linearized dynamics of nonlinearly coupled oscillators, such as the second-order Kuramoto model, which was previously used to investigate synchronization phenomena on power grids [39,40]. In the Appendix, we will demonstrate that the developed formalism may also be applied to such nonlinearly coupled systems.

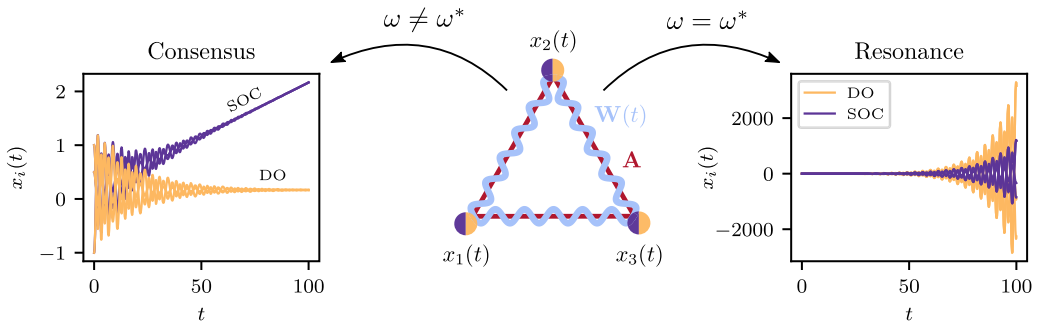

FIG. 1. Dynamics of the DO and SOC model for resonant and off-resonant coupling modulation. For ease of illustrations, we consider a small system of three agents, connected via a complete graph **A**. The coupling strength between any two agents is modulated time-periodically according to $\mathbf{W}(t) = f(t)\mathbf{A}$ [see Eq. (1)]. In the case of a static network **A** for $\omega = 0$, or sufficiently off-resonant modulations ($\omega \neq \omega^*$), the agents will reach a consensus in the limit of $t \to \infty$. In the case of the DO model velocities vanish and all agents come to rest in the same position. By contrast, for the SOC model consensus is defined as a state in which all agents move together as one cluster at a finite velocity. For resonant coupling modulations ($\omega = \omega_\alpha^*$) parametric excitation on a collective network level inhibits the establishment of global consensus states, and the agents' amplitudes diverge, as depicted in the right panel.

Note that the agents in the DO model achieve consensus due to the finite dissipation of $d > 0$ and the diffusive position coupling. Hence, the system evolves such that all agents will finally come to rest at the same position c and consensus is characterized as $x_i = c\ , \forall i$ and $\dot{x}_i(t \to \infty) = 0,\ \forall i$.

Subsequently, we investigate the effects of periodic coupling on the dynamics of the classical model for SOC on networks [15,18–27]. Here, agents do not dissipate energy ($d = 0$) but may establish consensus due to a velocity alignment mechanism, for $\mu > 0$ [see Eq. (2)], and consensus is reached if $|x_i - x_j| = 0\ , \forall i, j$ and $|\dot{x}_i - \dot{x}_j| = 0\ , \forall i, j$—a state with equal, but potentially finite, velocities [19]. In the following, we will show that both models are susceptible to time-periodic coupling, which inhibits the formation of consensus states. The presented formalism furthermore reveals an intimate relation between dissipation and velocity alignment, and their roles in consensus formation.

In the left panel of Fig. 1, the dynamics for off-resonant modulation is illustrated: both considered models reach consensus. While for the DO model a motionless consensus, via dissipation, emerges (orange lines), the consensus state of the SOC model preserves the total kinetic energy, and all agents move as a single cluster with a finite velocity (purple lines). In the case of resonant modulation consensus is inhibited for both models, and the agents' amplitudes increase exponentially as shown in the right panel of Fig. 1.

To proceed further, we express the general model, Eq. (2), in vectorial form:

$$\ddot{\boldsymbol{x}} + d(t)\dot{\boldsymbol{x}} = -\mathbb{L}(t)(\gamma \boldsymbol{x} + \mu \dot{\boldsymbol{x}}), \tag{3}$$

where $\mathbb{L}(t)$ denotes the time-dependent network Laplacian of the system. Analogous to the temporal coupling matrix, $\mathbf{W}(t)$, $\mathbb{L}(t)$ factorizes into the time-independent Laplacian $\mathbb{L}^{(0)}$ and the coupling modulation function $f(t)$, i.e., $\mathbb{L}(t) = \mathbb{L}^{(0)} f(t)$. The elements of $\mathbb{L}^{(0)}$ are obtained from the static backbone connectivity **A**:

$$\mathbb{L}_{ij}^{(0)} = \begin{cases} -A_{ij}, & i \neq j, \\ \sum_k A_{ik}, & i = j. \end{cases} \tag{4}$$

Note that the modulation $f(t)$ acts upon every connection of the static backbone network **A** simultaneously [32,33]. Therefore, the time-dependent eigenvalues of $\mathbb{L}(t)$, $\lambda_\alpha(t)$, can be expressed as $\lambda_\alpha(t) = \lambda_\alpha^{(0)} f(t)$ where $\{\lambda_\alpha^{(0)}\}$ is the set of eigenvalues of $\mathbb{L}^{(0)}$.

A spectral decomposition of Eq. (3), using $\mathbf{x}(t) = \sum_\alpha c_\alpha(t)\,\mathbf{u}_\alpha$, involving the eigenvectors of $\mathbb{L}^{(0)}$, $\mathbf{u}_\alpha$, gives rise to the following second-order differential equation:

$$\ddot{c}_\alpha + k(t)\dot{c}_\alpha + \gamma \lambda_\alpha(t) c_\alpha = 0, \tag{5}$$

where we have defined $k(t) = d(t) + \mu\lambda_\alpha(t)$, and c_α denotes the αth expansion coefficient of $\mathbf{x}(t)$ on the set of eigenvectors $\{\mathbf{u}_\alpha\}$.

The effect of a time-varying coupling on the dynamics of the system becomes now particularly evident: Eq. (5) describes the collective dynamics on the level of network modes, and manifests itself as a parametric oscillator [42]. Such oscillators are not excited by an explicit external force, but are susceptible to periodic variations of the system's parameters—the phenomenon of parametric resonance. Therefore, parametric oscillators cannot be driven out of a stable equilibrium, but existing deviations from such a stable state may be amplified exponentially by carefully tuned periodic modulations of $k(t)$ or $\lambda_\alpha(t)$. The expression of $k(t)$ reveals the analogy between dissipation $d > 0$, in the case of coupled damped harmonic oscillators, and the velocity alignment mechanism for the SOC model for $\mu > 0$. Both mechanisms may contribute to the damping of the αth mode, and will therefore influence the dynamics in similar ways.

In what follows, we treat Eq. (5) analytically and identify, for both model versions (DO and SOC), certain resonant modulation frequencies ω^* [see Eq. (1)], for which the corresponding networked systems cannot establish a global consensus. At a first glance this may come as a surprise: diffusively coupled agents, with $\mathbf{W}(t) > 0$, generally aim to assimilate; hence, one might indeed expect the emergence of consensus. Equation (5), however, suggests that periodically modulated coupling strengths translate into collective parametric resonance, which is characterized by an exponential growth of the agents' amplitudes. We establish an analytical link between the spectrum of the static Laplacian, $\lambda_\alpha^{(0)}$, and

the expected resonance frequencies ω_α^*. Finally, we quantify the exponential excitation for resonant modulation.

To obtain the set of resonance frequencies, we express Eq. (5) in a more suitable form, using the variable transformations

$$c_\alpha(t) = e^{-K(t)} q_\alpha(t), \tag{6}$$

$$K(t) = \frac{1}{2}\int_0^t k(t')dt'. \tag{7}$$

Substituting those into Eq. (5) yields

$$\ddot{q}_\alpha + \Omega_\alpha^2(t) q_\alpha = 0, \tag{8}$$

the Hill equation [43], with the time-dependent frequency $\Omega_\alpha(t)$, defined as

$$\Omega_\alpha^2(t) = \gamma\lambda_\alpha(t) - k^2(t)/4 - \dot{k}(t)/2. \tag{9}$$

Note that the time dependence of $\Omega_\alpha(t)$ results from a periodic modulation of the damping coefficient $d(t)$; from the αth eigenvalue of $\mathbb{L}(t)$, $\lambda_\alpha(t)$; or from both. Accordingly, Eq. (9) takes a different form for each of the two models (DO and SOC), which we will consider separately in the following.

A. Damped oscillator model

In the case of the DO model, we assume, for simplicity, a time-independent damping coefficient d. Then Eq. (9) becomes

$$\Omega_\alpha^2(t) = \gamma\lambda_\alpha^{(0)}[1 + h\sin(\omega t)] - d^2/4, \tag{10}$$

where we have used $\lambda_\alpha(t) = \lambda_\alpha^{(0)}[1 + h\sin(\omega t)]$. Defining $\omega_\alpha^2 = \gamma\lambda_\alpha^{(0)} - d^2/4$ yields

$$\ddot{q}_\alpha + \omega_\alpha^2\left[1 + \frac{\gamma\lambda_\alpha^{(0)} h}{\omega_\alpha^2}\sin(\omega t)\right] q_\alpha = 0, \tag{11}$$

such that parametric excitation, for the αth mode, is expected for ω_α^*:

$$\omega_\alpha^* = 2\omega_\alpha = 2\sqrt{\gamma\lambda_\alpha^{(0)} - \left(\frac{d}{2}\right)^2}, \tag{12}$$

which corresponds to twice the natural frequency of the system ω_α—as in the case of a one-dimensional parametric oscillator [36]. Note that not all eigenvalues $\lambda_\alpha^{(0)}$ are expected to give rise to a resonance, but only those eigenvalues which fulfill the following requirements:

$$4\gamma\lambda_\alpha^{(0)} > d^2, \tag{13}$$

$$\left|\frac{\gamma\lambda_\alpha^{(0)} h}{4\omega_\alpha}\right| > d. \tag{14}$$

Specifically, while Eq. (13) ensures that ω_α^*, in Eq. (12), is purely real, Eq. (14) yields an exponential growth of the induced oscillations (see below). Interestingly, as both conditions depend on the mode index α, only a subset of the modes may be activated by the periodic coupling depending on the values of d and h. More precisely, those conditions set a lower bound under which natural frequencies cannot be activated. In addition to locating the resonance frequencies ω_α^* in the system, it is instructive to quantify the exponential growth of the αth mode, due to resonant modulation.

To this end, we first assume small oscillation amplitudes in Eq. (11), i.e., $\gamma\lambda_\alpha^{(0)} h/\omega_\alpha^2 \ll 1$. Then the solution of Eq. (11) takes the form

$$q_\alpha(t) = a_\alpha(t)\cos[(\omega_\alpha + \varepsilon)t] + b_\alpha(t)\sin[(\omega_\alpha + \varepsilon)t], \tag{15}$$

where ε defines the detuning from ω_α^*. Note that this ansatz will not yield an exact solution to Eq. (11) as terms containing multiples of $(2\omega_\alpha + \epsilon)$ have been neglected. It is, however, sufficient in the case of small modulation amplitudes [36]. Inserting the expression for $q_\alpha(t)$ into Eq. (11), for the particular case of $\omega_\alpha^* = 2\omega_\alpha + \epsilon$, and neglecting terms of order $\mathcal{O}(h^2)$, yields

$$\begin{aligned} -2\dot{a}_\alpha + a_\alpha\frac{\gamma\lambda_\alpha^{(0)} h}{2\omega_\alpha} - 2\varepsilon b_\alpha &= 0, \\ 2\dot{b}_\alpha + b_\alpha\frac{\gamma\lambda_\alpha^{(0)} h}{2\omega_\alpha} - 2\varepsilon a_\alpha &= 0. \end{aligned} \tag{16}$$

We search the solutions to Eqs. (16) in the form of $a_\alpha(t)$ and $b_\alpha(t) \sim e^{s_\alpha t}$, respectively, which yields the following expression for the exponent s_α:

$$s_\alpha^2 = \left[\frac{\gamma\lambda_\alpha^{(0)} h}{4\omega_\alpha}\right]^2 - \varepsilon^2 = \left[\frac{\gamma\lambda_\alpha^{(0)} h}{4\sqrt{\gamma\lambda_\alpha^{(0)} - d^2/4}}\right]^2 - \varepsilon^2. \tag{17}$$

Hence, resonance for the αth mode is expected on the following interval of ϵ:

$$-\frac{\gamma\lambda_\alpha^{(0)} h}{4\sqrt{\gamma\lambda_\alpha^{(0)} - d^2/4}} < \varepsilon < \frac{\gamma\lambda_\alpha^{(0)} h}{4\sqrt{\gamma\lambda_\alpha^{(0)} - d^2/4}}, \tag{18}$$

centered around the resonance frequency ω_α^*. Note that the width of the interval depends linearly on h, such that the excitation region is increased for larger modulation amplitudes. In the case of perfectly resonant modulation ($\varepsilon = 0$) the amplitudes $a_\alpha(t)$ and $b_\alpha(t)$ are expected to grow exponentially as $e^{s_\alpha t}$. Resubstituting this into the initial expression for the expansion coefficients yields $c_\alpha(t) \propto e^{(s_\alpha - d)t}$, from which condition (14) is derived.

B. Second-order consensus model

In a similar manner, we may approach the SOC model, which is discussed in the following. Here, we consider Eq. (3) without damping ($d = 0$) and with diffusive velocity coupling ($\mu > 0$). Starting again from Eq. (9), for $k(t) = \mu\lambda_\alpha^{(0)}[1 + h\sin(\omega t)]$, we get

$$\begin{aligned} \Omega_\alpha^2(t) = \gamma\lambda_\alpha^{(0)} &- \left(\frac{\mu\lambda_\alpha^{(0)}}{2}\right)^2 \\ &+ \left[\gamma\lambda_\alpha^{(0)} h - 2h\left(\frac{\mu\lambda_\alpha^{(0)}}{2}\right)^2\right]\sin(\omega t) \\ &- \frac{h\omega\mu\lambda_\alpha^{(0)}}{2}\cos(\omega t) - \left(\frac{h\mu\lambda_\alpha^{(0)}}{2}\right)^2\sin^2(\omega t). \end{aligned} \tag{19}$$

Small modulation amplitudes, $h \ll 1$, allow us to neglect terms of the order $\mathcal{O}(h^2)$ in the expression of $\Omega_\alpha^2(t)$.

Combining the linear cosine and sine terms yields

$$\Omega_\alpha^2(t) \simeq \omega_\alpha^2\left(1+\frac{B}{\omega_\alpha^2}\sin(\omega t+\varphi)\right) \tag{20}$$

with

$$\omega_\alpha^2 = \gamma\lambda_\alpha^{(0)} - \left(\frac{\mu\lambda_\alpha^{(0)}}{2}\right)^2, \tag{21}$$

$$B = h\sqrt{\left(\frac{\omega\mu\lambda_\alpha^{(0)}}{2}\right)^2 + \left(\gamma\lambda_\alpha^{(0)} - \frac{\left(\mu\lambda_\alpha^{(0)}\right)^2}{2}\right)^2}, \tag{22}$$

and

$$\varphi = \tan^{-1}\left(\frac{\omega\mu\lambda_\alpha^{(0)}}{2\gamma\lambda_\alpha^{(0)} - \left(\mu\lambda_\alpha^{(0)}\right)^2}\right). \tag{23}$$

As in the previous case of the DO model, the resonance frequency corresponds to twice the natural frequency of the system ω_α, i.e.,

$$\omega_\alpha^* = 2\omega_\alpha = 2\sqrt{\gamma\lambda_\alpha^{(0)} - \left(\frac{\mu\lambda_\alpha^{(0)}}{2}\right)^2}, \tag{24}$$

and we get

$$s_\alpha^2 = \left[\frac{B}{4\omega_\alpha}\right]^2 - \varepsilon^2, \tag{25}$$

where $c_\alpha(t)$ is expected to grow exponentially if $s_\alpha t - K(t) > 0$. The detuning range for the SOC is limited to the interval $-B/(4\omega_\alpha) < \epsilon < B/(4\omega_\alpha)$ around ω_α^*. Evaluating the integral in Eq. (7) yields

$$K(t) = \frac{\mu\lambda_\alpha^{(0)}}{2}\left\{t + \frac{h}{\omega}[1-\cos(\omega t)]\right\}, \tag{26}$$

which reduces for $h \ll 1$ to

$$K(t) \simeq \frac{\mu\lambda_\alpha^{(0)}}{2}t. \tag{27}$$

Resonances are therefore expected if the following two inequalities are fulfilled:

$$B\omega_\alpha - 2\mu\lambda_\alpha^{(0)} > 0 \tag{28}$$

and

$$\gamma - \frac{\mu^2}{4}\lambda_\alpha^{(0)} > 0. \tag{29}$$

Note that, as with γ for the DO model, the velocity alignment mechanism, controlled by the parameter μ, is hampering the emergence of parametric resonance and therefore fosters consensus.

The presented results are rather general. They allow us to determine the resonance frequencies ω_α^* for systems on arbitrary static backbone structures $\mathbf{A}$, where the coupling between agents is modulated by a periodic function $f(t)$ of small amplitudes. In the following, we investigate those resonance effects for both models and on different backbone networks. While the eigenvalues $\lambda_\alpha^{(0)}$ of $\mathbb{L}^{(0)}$, required for the determination of $\{\omega_\alpha^*\}$, can be obtained analytically for simple regular graphs, they need to be determined numerically for more complex or random networks.

III. NUMERICAL RESULTS

In order to validate the theoretical analysis we perform numerical simulations. As suggested by the theory, the agents in both models will or will not reach a global consensus, depending on the modulation frequency ω. To detect the corresponding ranges of resonance numerically, we shall proceed as follows. We integrate Eqs. (3), using a fourth-order Runge-Kutta scheme [44], by which we obtain the time evolution of the system, $\mathbf{x}(t)$, for a specific modulation frequency ω. Based on $\mathbf{x}(t)$, there are, in principle, several possibilities to detect a resonance. Here, we chose to compute the integral $\int_0^T \mathbf{x}^2(t)\,dt$, up to a fixed time T. This quantity is averaged over multiple realizations, with random starting vectors $\mathbf{x}(0)$, to ensure that the observed resonances are stable with respect to different initial conditions. Finally, this yields

$$\mathcal{A}(\omega) = \left\langle \int_0^T \mathbf{x}^2(t)\,dt \right\rangle_{\{\mathrm{IC}\}}, \tag{30}$$

which quantifies the response of the system to a specific modulation frequency ω, in terms of the agents' integrated squared amplitudes. In such a spectrum, $\mathcal{A}(\omega)$, resonances appear as pronounced peaks, while regions of consensus are flat. Note that the value of $\mathcal{A}(0)$ corresponds to the case of a static network $\mathbf{A}$ [see Eq. (1)]. Without loss of generality we initialize both models as resting nonconsensus states, i.e., we set the state variables at time $t = 0$ randomly on the interval $x_i(0) \in \mathcal{I}_{\mathrm{init}}$, and assume vanishing initial velocities $\dot{x}_i(0) = 0, \quad \forall i$. Unless indicated differently we take $\mathcal{I}_{\mathrm{init}} = [-1, 1]$, $h = 0.2$ and set $(d = 0.01, \gamma = 1)$ and $(\gamma = 1, \mu = 0.01)$ for the DO and SOC model, respectively, for reasons of comparability between both models. As a consequence of this choice, the predicted resonance frequencies are similar for both models, and it is ensured that the conditions (13) and (14) and the conditions (28) and (29) are satisfied. In the following we discuss our theoretical results on complete graphs, on ring networks, and finally on random Erdős-Rényi (ER) networks [45].

A. Amplitude growth

In a first step, we check the theoretical predictions with respect to the exponential growth of the system's amplitudes in the case of resonant modulation. Here, we consider, for simplicity, the case without both damping ($d = 0$) and velocity alignment ($\mu = 0$), such that the two considered models coincide: the expressions for the resonance frequencies [see Eqs. (12) and (24)] yield $\omega_\alpha^* = 2\sqrt{\gamma\lambda_\alpha^{(0)}}$, and the exponent s_α becomes

$$s_\alpha = \frac{h\sqrt{\gamma\lambda_\alpha^{(0)}}}{4}. \tag{31}$$

The case of such parametric excitation is shown in Fig. 2, for a complete graph of $n = 100$ nodes, where the single resonance is obtained as $\omega^* = 20$. For clarity of depiction, the trajectory and the local maximum values of a single node ($i = 1$) are shown in green. The trajectories $x_j(t)$ of the remaining agents are colored in gray. Clearly, for resonant modulation the nodes' amplitudes increase exponentially over time. The

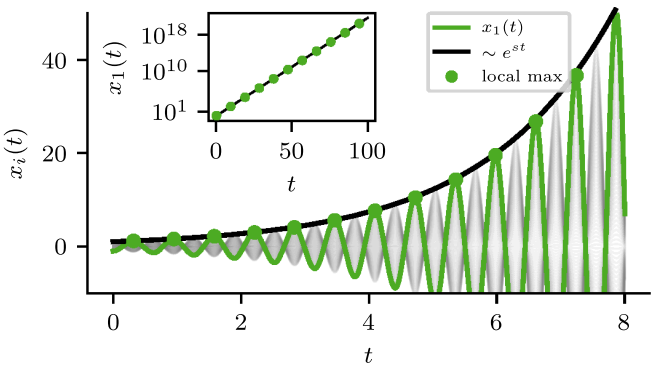

FIG. 2. Amplitude growth for resonant modulation with $\omega = \omega^*$ and $d = \mu = 0$. The exponential growth of the agents' amplitudes is quantitatively captured by the time evolution of the αth expansion coefficient $c_\alpha(t) \sim e^{st}$ (black line). The green trajectory corresponds to the time evolution of a single agent i, and its local maximum values are depicted as green dots. The inset shows the exponential growth as a subset of local maximum values of the same agent (green dots) and $c_\alpha(t)$ (black line), over many orders of magnitude. The results shown are for a complete graph with $n = 100$ nodes.

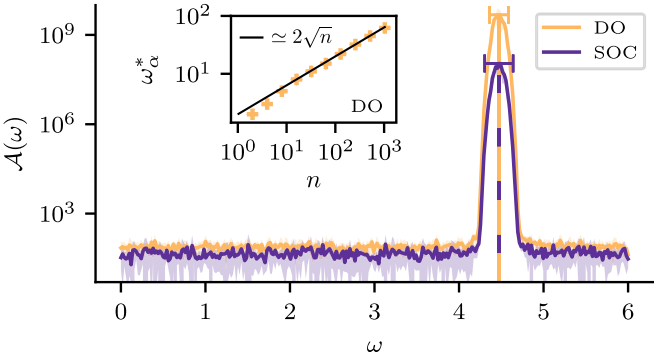

FIG. 3. Resonance on a complete graph. The vertical orange and dashed purple lines locate the predicted resonance frequency ω^* for each model on a complete graph of $n = 5$ nodes. The orange and purple spectra correspond to the DO and SOC model, respectively, on the interval $\omega \in [0, 6]$. The spectra are computed as averages over ten random initial conditions, and the shaded areas show the corresponding standard deviations. The widths of the resonance peaks are approximately captured by the interval of ε around ω^* [see Eqs. (18) and (25)]. The inset shows, for the DO model, the theoretically predicted values of ω^* (black line), and as extracted from simulations (orange crosses), as functions of the system size.

growth is well captured by $c_\alpha(t) \sim e^{st}$ (black line), where s is given in Eq. (31). As the inset of Fig. 2 demonstrates, the behavior is not only well described for short times, but the approximation also holds for larger times, spanning many orders of magnitude.

B. Complete graphs

To verify the theoretical analysis predicting the values of resonance frequencies, we first consider complete graphs, or all-to-all connected networks—a general network topology often considered in studies of coupled oscillators [40]. The eigenvalues of $\mathbb{L}^{(0)}$ for a complete graph are given as $\lambda_0 = 0$ and $\lambda_1 = n$, where λ_1 has the algebraic multiplicity $n - 1$ [46].

Based on Eqs. (12) and (21), we expect parametric resonance around the single frequency

$$\omega^* = 2\sqrt{\gamma n - \left(\frac{d}{2}\right)^2} \tag{32}$$

for the DO model and

$$\omega^* = 2\sqrt{\gamma n - \left(\frac{\mu n}{2}\right)^2} \tag{33}$$

in the case of the SOC model.

In Fig. 3, we depict the corresponding resonance spectra on a complete graph of $n = 5$ nodes. Here and in all subsequent figures the orange and purple lines depict the spectra of the DO and SOC model, respectively. Vertical lines locate the predicted values for ω^*_α, colored according to the associated model. For both models, the single peaks of integrated square amplitudes $\mathcal{A}(\omega)$ are predicted remarkably well by the theoretical values of ω^*. Furthermore, the finite widths of the peaks are approximately captured by the theoretical bounds of detuning ε.

The thermodynamic limit, $n \to \infty$, yields different behaviors for both models. For fixed values of μ and γ, no resonance is expected for the SOC model, as the resonance conditions are violated for large n. Instead, in the case of the DO model the damping coefficient does not influence the expression for ω^* significantly. Hence, the resonance frequency is well described by $\omega^*_\infty \simeq 2\sqrt{n}$, which is supported by numerical simulations for network sizes up to $n = 1000$ [see inset of Fig. 3(a)]. For growing system sizes, the establishment of a global consensus, in the DO model, is therefore increasingly robust against low frequency modulations in $f(t)$, and only high frequency components may parametrically excite the system and inhibit consensus.

C. Rings

In contrast to complete graphs, the Laplacian spectrum of a ring network may contain more than two distinct eigenvalues, which may generally lead to multiple resonances. The set $\{\lambda^{(0)}_\alpha\}$ distributes over the interval $\lambda^{(0)}_\alpha \in [0, 4]$, and the eigenvalues are given as

$$\lambda^{(0)}_\alpha = 2 - 2\cos(k_\alpha), \tag{34}$$

with $k_\alpha = 2\pi(\alpha - 1)/n$ [46]. This leads to the following expressions for the resonance frequencies:

$$\omega^*_\alpha = 2\sqrt{2 - 2\cos(k_\alpha) - \left(\frac{d}{2}\right)^2} \tag{35}$$

in the case of the DO model, and likewise

$$\omega^*_\alpha = 2\sqrt{2 - \mu^2 + (2\mu - 2)\cos(k_\alpha) - \mu^2\cos^2(k_\alpha)} \tag{36}$$

for the SOC model. Note that for a ring network of $n = 5$ nodes both distinct eigenvalues $\lambda^{(0)}_\alpha > 0$ give rise to valid resonance frequencies ω^*_α, i.e., all resonance conditions are satisfied for $d = \mu = 0.01$. The corresponding spectra are depicted in Fig. 4(a), where both resonances show up as pronounced peaks, matched by their theoretical predictions.

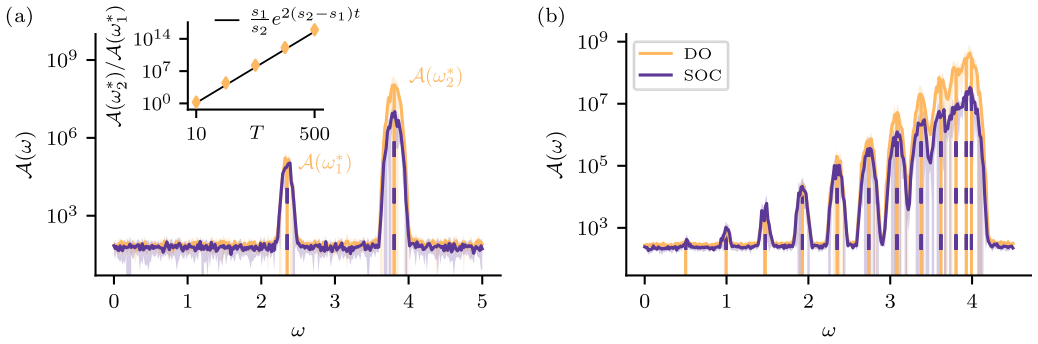

FIG. 4. Resonances on ring networks. The orange and dashed purple vertical lines locate the analytically predicted resonance frequencies for both models, on a ring network of $n = 5$ (a) and $n = 25$ (b) nodes, respectively. The resonance spectra are computed as averages over ten random initial conditions and a simulation time of $T = 100$. The inset in panel (a) depicts the ratio $\mathcal{A}(\omega_2^*)/\mathcal{A}(\omega_1^*)$ for the DO model, as a function of the simulation time T (orange rhombuses). The time-dependent ratio is well described by $e^{2(s_2-s_1)t}$ (black line), where s_1 and s_2 are computed using ω_1 and ω_2 [see Eq. (17)].

For the chosen simulation time of $T = 100$, the heights of the resonance peaks, $\mathcal{A}(\omega_1^*)$ and $\mathcal{A}(\omega_2^*)$, are separated by several orders of magnitude, where the separation is larger in the case of the DO model. In the inset of Fig. 4(a), we demonstrate, for the DO model, that the ratio of observed peak heights is well captured by the theory. Taking into account the different exponential growth rates s_α for both resonances, the ratio can, for large t, be approximated as $\int c_2^2 dt / \int c_1^2 dt \sim (s_1/s_2)\, e^{2(s_2-s_1)t}$ (black line), obtained from Eq. (17), and well describes the numerical results, over many orders of magnitude.

In Fig. 4(b) we show the resonance spectra for larger ring networks of $n = 25$ nodes, where an important consequence of the bounded Laplacian spectrum becomes apparent. At odds with the behavior of the DO model on complete graphs, increasing the number of nodes for ring networks does not increase the highest resonance frequency beyond all limits. Instead, for $n \to \infty$, the bounded intervals of resonance frequencies are gradually filled with resonance peaks, as suggested by Eqs. (34). Once two resonant frequencies are sufficiently close to each other, i.e., within their respective ε ranges, also intermediate frequencies may parametrically excite the system, such that the resonance spectra become quasicontinuous ones. This effect occurs for higher modulation frequencies, $3 < \omega \leqslant 4$, where the increased values of $\mathcal{A}(\omega)$, between two predicted resonance frequencies ω_α^* and $\omega_{\alpha+1}^*$, indicate a partially off-resonant excitation of the system.

D. Random networks

Finally we demonstrate that the theory holds on random networks, i.e., we confirm that resonance frequencies (based on $\mathbb{L}^{(0)}$) can be reliably predicted on networks with disorder. In the previous cases of regular ring networks and complete graphs, the Laplacian spectra were given analytically. This is not the case for random networks, and the corresponding eigenvalues, λ_α, need to be determined numerically.

In Fig. 5, we depict the resonance spectra for two ER networks of $n = 10$ [panel (a)] and $n = 100$ [panel (b)] nodes. Especially, in the former case, the random network structure is reflected in the rather irregular positions of the resonance peaks—an observation which is directly related to the random spectrum of the corresponding Laplacian $\mathbb{L}^{(0)}$. Nevertheless, the resonances for both models are successfully predicted by Eqs. (12) and (24).

In the case of the larger ER network [see panel (b) of Fig. 5], the resonance frequencies are very close to each other, such that the single vertical lines are barely distinguishable.

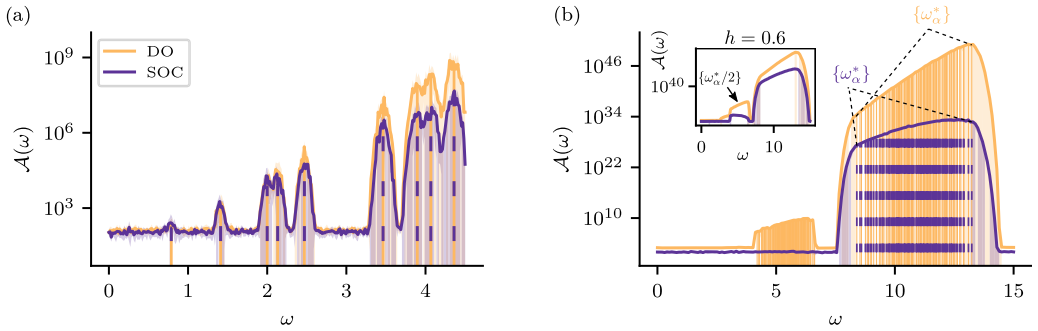

FIG. 5. Resonances on Erdős-Rényi networks. The orange and dashed purple vertical lines locate the analytically predicted resonance frequencies ω_α^* for both models on Erdős-Rényi networks of $n = 25$ (a) and $n = 100$ (b) nodes, respectively. The spectra are averaged over ten random initial conditions, and the shaded areas show the corresponding standard deviations. In panel (b) the modulation amplitude is $h = 0.4$. The inset of panel (b) shows the spectrum obtained for an even larger modulation amplitude $h = 0.6$, where half resonant frequencies excite the system, also for the SOC model.

The overlapping detuning ranges ϵ, hence, lead to a quasi-continuous excitation of the system on the whole interval of roughly $\omega \in [8, 13]$ for both models. Interestingly, the resonance spectrum of the DO model shows a further feature, known for general parametric oscillators: the excitation of the system at half the resonance frequency [36]. As we show in the inset of Fig. 5, this effect becomes increasingly pronounced for larger modulation amplitudes ($h = 0.6$), and is not limited to the DO model, but also appears for the SOC model.

IV. SUMMARY AND CONCLUSIONS

In this paper, we studied parametric resonances in a general consensus model of networked agents, which we discussed in two different settings: (i) a model for damped harmonic oscillators and (ii) the well established model for second-order consensus formation, without dissipation and with velocity alignment. We considered those models for time-periodic coupling modulations and found that, for certain intermediate time scales of such modulation, the collective dynamics is not captured by the time-averaged coupling $\mathbf{A} = \langle \mathbf{W}(t) \rangle_t$, which would lead to a global consensus state. Instead, parametric resonance is induced on a collective level, where single network modes are excited and the emergence of consensus is inhibited. The developed formalism correctly predicts those resonance frequencies within the theory of parametric resonance, which we extended to the domain of networks with time-varying coupling. As we demonstrated, resonant modulation gives rise to exponentially growing mode amplitudes, which can be quantified in terms of the associated eigenvalues of the static Laplacian $\mathbb{L}^{(0)}$. In this context, both dissipation and velocity alignment counteract the excitation of the system, and therefore foster the establishment of global consensus states.

In comparison, both considered models, DO and SOC, are similarly susceptible to time-periodic coupling modulations. However, for increasing resonance frequencies, the excitation of the DO model is stronger compared to the SOC model, as suggested by numerical simulations. For small system sizes and rather weak dissipation, as well as weak velocity alignment, the expected resonance frequencies are in close vicinity. Using the example of complete graphs, we illustrated that this generally changes for large networks. Increasingly large Laplacian eigenvalues do not yield resonances in the SOC model. This emphasizes the enhanced positive effect of velocity alignment on consensus formation, compared to dissipation.

Interestingly, we found that the developed formalism also holds on networks of nonlinearly coupled second-order Kuramoto oscillators, close to a synchronization fixed point. It correctly predicts modulation frequencies for which the synchronized state becomes unstable. This does not yield exponentially growing but finite oscillation amplitudes. Periodic coupling modulations, far from any synchronous fixed point, might also impact the critical coupling strength for the second-order Kuramoto model, which is a promising line of future research.

Our paper might have important implications for the robustness of second-order consensus algorithms, applied in real systems. For example, in order to disrupt consensus states within networked vehicular platoons or cooperating autonomous robots, signals, which periodically weaken the units' sensors, may be used. Parametric resonance might furthermore be used to infer characteristic networks features, in cases where the probing of the system is not localized on certain nodes, but performed on the overall coupling.

ACKNOWLEDGMENTS

This work was developed within the scope of IRTG 1740/TRP Project No. 2015/50122-0 and funded by the Deutsche Forschungsgemeinschaft and FAPESP and by the Swiss National Science Foundation under Grant No. 200020_182050. We thank Adrian Pacheco, Jörg Nötel, and Thomas Peron for fruitful discussions and helpful comments on the paper.

APPENDIX: NONLINEAR OSCILLATORS

In the main text we considered (linear) diffusively coupled second-order consensus models. However, Eq. (3) may also be regarded as the linearization of nonlinearly coupled oscillators, to which the theoretical framework may be applied, if the dynamics close to a fixed point is considered. Traditionally, one of the most studied models of this kind is the Kuramoto model [37]. Specifically, second-order Kuramoto models were mostly used to investigate synchronization phenomena in power grids [39,40].

Exchanging the diffusive coupling by a sinusoidal one, setting $\mu = 0$ and switching to the common notation for phase oscillators, i.e., $x_i \to \phi_i$, Eq. (3) yields the second-order Kuramoto model as

$$\ddot{\phi}_i + d\,\dot{\phi}_i = \omega_i - \sum_{j=1}^{N} W_{ij}(t)\sin(\phi_i - \phi_j), \tag{A1}$$

where we have additionally introduced the natural frequency ω_i of oscillator i. Without loss of generality, we take $\sum_i \omega_i = 0$, which yields a synchronous state with $\dot{\phi}_i = 0\ \forall i$. Furthermore we assume that Eq. (A1) has a stable fixed point $\phi_{i,0}$ for a specific backbone network $\mathbf{A}$; hence,

$$\omega_i = \sum_{j=1}^{N} W_{ij}(t)\sin(\phi_{i,0} - \phi_{j,0}). \tag{A2}$$

For small modulation amplitudes in $f(t)$, $h \ll 1$, the dynamics of $\delta\phi_i(t) = \phi_i(t) - \phi_{i,0}$ is captured by the linearization of Eq. (A1), which yields

$$\delta\ddot{\phi}_i + d\,\delta\dot{\phi}_i = -\sum_{j=1}^{N} W_{ij}(t)\cos(\phi_{i,0} - \phi_{j,0})(\delta\phi_{i,0} - \delta\phi_{j,0}), \tag{A3}$$

and

$$\delta\ddot{\boldsymbol{\phi}} + d\delta\dot{\boldsymbol{\phi}} = -\mathbb{L}(t;\boldsymbol{\phi}_0)\,\delta\boldsymbol{\phi} \tag{A4}$$

in vectorial form. In the latter equation $\mathbb{L}(t;\boldsymbol{\phi}_0)$ denotes a Laplacian matrix, weighted by the cosine of angle differences at the fixed point $\boldsymbol{\phi}_0$. Therefore, the relations derived in Sec. II still hold—where $\{\lambda_\alpha^{(0)}\}$ now corresponds to the eigenvalue spectrum of the weighted Laplacian $\mathbb{L}(t;\boldsymbol{\phi}_0)$. Note that in

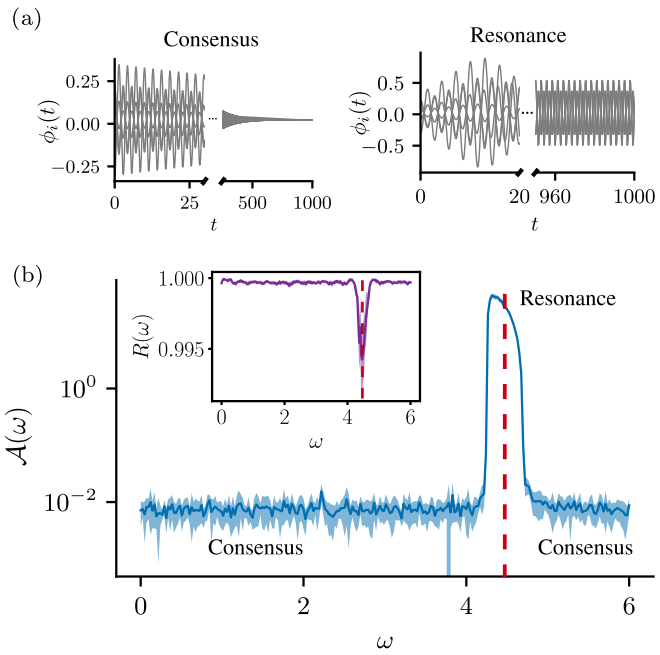

FIG. 6. Resonance for the second-order Kuramoto model. Panel (a) shows the time evolution of the second-order Kuramoto model for off-resonant (left) and resonant ($\omega^* \simeq 4.3$) coupling modulation (right). Panel (b) depicts the corresponding spectrum $\mathcal{A}(\omega)$ (blue line). The red dashed line locates the predicted resonance frequency ω^* for a complete graph of $n = 5$ nodes close to the consensus fixed point. The shaded blue area shows the standard deviation of $\mathcal{A}(\omega)$ for ten random initial conditions. The initial interval was set to $\mathcal{I}_{\text{init}} = [-0.01, 0.01]$. The inset shows the order parameter R plotted against the modulation frequency ω.

the specific case where $\omega_i = 0$, $\forall\, i$, one trivial synchronized state satisfies $\phi_{0,i} = \phi_{0,j}$, $\forall i, j$. In this particular case the weighted Laplacian reduces to the one used in the linear models [Eq. (3)], i.e., we have $\mathbb{L}(t, \boldsymbol{\phi}_0) = \mathbb{L}(t)$.

The right panel of Fig. 6(a) shows the time evolution of the phases ϕ_i for resonant modulation ($\omega = \omega^*$), on a complete graph of $n = 5$ nodes. As expected, in the case of resonance, consensus is inhibited. In contrast to the linear models (DO and SOC), however, oscillation amplitudes stay finite due to the boundedness of the sinusoidal coupling, which inhibits an arbitrarily large excitation of the system. For off-resonant modulation, instead, agents reach a global consensus, as shown in the left panel of Fig. 6(a), similar to the linear models (see Fig. 1). This behavior is consistent over the whole range of relevant modulation frequencies as shown in Fig. 6(b), where a pronounced peak appears for the same frequency as predicted for the DO model (see Fig. 3). Note that the linearization of the sinusoidal coupling only holds for the dynamics close to a fixed point. For our numerical simulations, we therefore reduce the width of the initial interval of $\phi_i(0)$ to $\mathcal{I}_{\text{init}} = [-0.01, 0.01]$ to study the resonance close to the consensus point.

Traditionally, the degree of synchronization of the Kuramoto model is discussed in terms of the order parameter $R = |N^{-1} \sum_j e^{i\phi_j}|$ [47], where $|\cdot|$ refers to the module. In the inset of Fig. 6(b), we complement the resonance spectrum $\mathcal{A}(\omega)$ by a numerical evaluation of the order parameter R, for the same ω range. We find that there is a (small) decrease in R, around the predicted resonance frequency, shown by the red dashed line, which can be explained as follows. For synchronized consensus states, as the one depicted in the left panel of Fig. 6(a), all agents converge to the same state [because we take $\omega_i = 0$, $\forall i$; in the most general case, agents' deviations ($\delta\phi_i$) instead tend to the same value]. Accordingly, the resulting values of R are close to 1. Instead, for resonant modulation, around $\omega^* \simeq 4.3$, the agents oscillate with constant amplitudes. However, parametric excitation can only happen for finite phase differences, such that oscillations are not in phase, which reduces the order parameter $R < 1$. Note that the observed effect is small, due to the small system size of $n = 5$ oscillators.

[1] D. S. Bassett and O. Sporns, Nat. Neurosci. **20**, 353 (2017).
[2] E. M. Izhikevich, *Dynamical Systems in Neuroscience* (MIT Press, Cambridge, MA, 2007).
[3] S. B. Rosenthal, C. R. Twomey, A. T. Hartnett, H. S. Wu, and I. D. Couzin, Proc. Natl. Acad. Sci. USA **112**, 4690 (2015).
[4] Y. Katz, K. Tunstrøm, C. C. Ioannou, C. Huepe, and I. D. Couzin, Proc. Natl. Acad. Sci. USA **108**, 18720 (2011).
[5] H. G. Tanner, A. Jadbabaie, and G. J. Pappas, in *Proceedings of the 42nd IEEE International Conference on Decision and Control* (IEEE, New York, 2003), Vol. 2, pp. 2010–2015.
[6] V. Gupta, B. Hassibi, and R. M. Murray, in *Proceedings of the 42nd IEEE International Conference on Decision and Control* (IEEE, New York, 2003), Vol. 1, pp. 504–509.
[7] A. Rodriguez-Angeles and H. Nijmeijer, in *Proceedings of the 42nd IEEE International Conference on Decision and Control* (IEEE, New York, 2003), Vol. 2, pp. 1514–1519.
[8] J. Werfel, K. Petersen, and R. Nagpal, Science **343**, 754 (2014).
[9] M. A. Porter and J. P. Gleeson, in *Dynamical Systems on Dynamical Networks*, Frontiers in Applied Dynamical Systems: Reviews and Tutorials (Springer International Publishing, Cham, Switzerland, 2016), Vol. 4, pp. 49–51.
[10] M. H. DeGroot, J. Am. Stat. Assoc. **69**, 118 (1974).
[11] A. Baronchelli, R. Soc. Open Sci. **5**, 172189 (2018).
[12] C. Castellano, S. Fortunato, and V. Loreto, Rev. Mod. Phys. **81**, 591 (2009).
[13] I. Couzin, Nature (London) **445**, 715 (2007).
[14] M. Hechter and K.-D. Opp, *Social Norms* (Russell Sage Foundation, New York, 2001).
[15] W. Ren, R. W. Beard, and E. M. Atkins, IEEE Control Syst. Mag. **27**, 71 (2007).
[16] H.-T. Zhang, Z. Cheng, G. Chen, and C. Li, IEEE Trans. Circ. Syst. I **62**, 1599 (2015).
[17] W. Ren, R. W. Beard, and E. M. Atkins, in *Proceedings of the 2005 American Control Conference* (IEEE, New York, 2005), pp. 1859–1864.

[18] W. Ren and E. Atkins, in *Proceedings of the AIAA Guidance, Navigation, and Control Conference and Exhibit*, 2005 (unpublished), p. 6238.
[19] W. Ren and E. Atkins, Int. J. Robust Nonlin. Control **17**, 1002 (2007).
[20] W. Yang, A. L. Bertozzi, and X. Wang, in *Proceedings of the 2008 47th IEEE Conference on Decision and Control* (IEEE, New York, 2008), pp. 2926–2931.
[21] J. Qin, C. Yu, and S. Hirche, IEEE Trans. Ind. Infor. **8**, 986 (2012).
[22] W. Ren, in *Proceedings of the 2007 American Control Conference* (IEEE, New York, 2007), pp. 1431–1436.
[23] W. Yu, G. Chen, M. Cao, and J. Kurths, IEEE Trans. Syst., Man, Cybern., Part B **40**, 881 (2009).
[24] W. Yu, G. Chen, and M. Cao, Automatica **46**, 1089 (2010).
[25] D. Goldin and J. Raisch, Asian J. Control **16**, 30 (2014).
[26] X. Ai, S. Song, and K. You, Automatica **68**, 329 (2016).
[27] J. Hu, G. Chen, and H.-X. Li, in *Proceedings of the 30th Chinese Control Conference* (IEEE, New York, 2011), pp. 4819–4824.
[28] W. Ren and R. W. Beard, IEEE Trans. Autom. Control **50**, 655 (2005).
[29] A. Pikovsky, J. Kurths, M. Rosenblum, and J. Kurths, *Synchronization: A Universal Concept in Nonlinear Sciences* (Cambridge University Press, Cambridge, England, 2003), Vol. 12.
[30] A. Arenas, A. Díaz-Guilera, J. Kurths, Y. Moreno, and C. Zhou, Phys. Rep. **469**, 93 (2008).
[31] L. Kocarev, *Consensus and Synchronization in Complex Networks* (Springer, New York, 2013).
[32] S. Li, X. Wang, and S. Guan, New J. Phys. **20**, 113013 (2018).
[33] S. Li, N. Sun, L. Chen, and X. Wang, Phys. Rev. E **98**, 012304 (2018).
[34] H. G. Oral, E. Mallada, and D. F. Gayme, in *Proceedings of the 2017 IEEE 56th Annual Conference on Decision and Control (CDC)* (IEEE, New York, 2017), pp. 1688–1694.
[35] M. Zhan, S. Liu, and Z. He, PLoS ONE **8**, e82161 (2013).
[36] L. D. Landau and E. M. Lifschitz, *Lehrbuch der Theoretischen Physik, Band I, Mechanik*, 11th ed. (Akademie, Berlin, 1984), Vol. 1.
[37] Y. Kuramoto, in *International Symposium on Mathematical Problems in Theoretical Physics* (Springer, New York, 1975), pp. 420–422.
[38] H.-A. Tanaka, A. J. Lichtenberg, and S. Oishi, Physica D **100**, 279 (1997).
[39] F. Dörfler, M. Chertkov, and F. Bullo, Proc. Natl. Acad. Sci. USA **110**, 2005 (2013).
[40] F. A. Rodrigues, T. K. D. Peron, P. Ji, and J. Kurths, Phys. Rep. **610**, 1 (2016).
[41] T. W. Grunberg and D. F. Gayme, IEEE Trans. Control Network Sys. **5**, 456 (2018).
[42] L. Turyn, Q. Appl. Math. **51**, 389 (1993).
[43] G. W. Hill, Acta Math. **8**, 1 (1886).
[44] W. H. Press, S. A. Teukolsky, W. T. Vetterling, and B. P. Flannery, *Numerical Recipes in Pascal: The Art of Scientific Computing* (Cambridge University Press, Cambridge, UK, 1989), Vol. 1.
[45] P. Erdős and A. Rényi, Publ. Math. Inst. Hung. Acad. Sci. **5**, 17 (1960).
[46] A. E. Brouwer and W. H. Haemers, *Spectra of Graphs* (Springer, New York, 2011).
[47] Y. Kuramoto, *Chemical Oscillations, Waves, and Turbulence* (Courier, New York, 2003).